ECCOMAS Congress 2016
VII European Congress on Computational Methods in Applied Sciences and Engineering
M. Papadrakakis, V. Papadopoulos, G. Stefanou, V. Plevris (eds.)
Crete Island, Greece, 5–10 June 2016

RECOVERY OF DIFFERENTIATION/INTEGRATION COMPATIBILITY OF MESHLESS OPERATORS VIA LOCAL ADAPTATION OF THE POINT CLOUD IN THE CONTEXT OF NODAL INTEGRATION

Gabriel Fougeron[1,2], **Guillaume Pierrot**[1] **and Denis Aubry**[2]

[1]ESI-Group
99 Rue des Solets, Parc d'affaires SILIC, 94513 RUNGIS CEDEX, FRANCE
e-mail: {gabriel.fougeron,guillaume.pierrot}@esi-group.com

[2]CentraleSupélec Laboratoire MSSMat - UMR CNRS 8579
Grande Voie des Vignes 92290 CHATENAY-MALABRY, FRANCE
e-mail: denis.aubry@ecp.fr

Keywords: Meshless methods, Nodal integration, SPH, Advection, Diffusion.

Abstract. *Standard SPH methods are very attractive to simulate complex flow problems thanks to their robustness and ease of implementation, but often suffer from poor precision regarding point-wise stress computation or stability issues characterized by a loss of quality of the point cloud (particle clumping, formation of voids).*

In this paper, we recall an operator-based framework for the description of meshless discretizations using nodal integration. Using this framework, we are able to define a dual gradient inspired by the integration by parts formula, clarify its role in the discretization of a simple diffusion problem and specify sufficient conditions to satisfy the patch test. For symmetric discretizations, we show that one of these conditions reduces to a discrete version of Stokes' theorem, which we call differentiation/integration compatibility of meshless operators.

Our earlier work [22] focused on the recovery of these compatibility conditions via the modification of gradient coefficients. In a companion presentation [23], we extend the analysis to the concept of element-based integration and investigate the possibility of a one-shot solution algorithm, jointly solving for both compatibility and pressure.

The present work however is an attempt at achieving compatibility while keeping the computational simplicity of SPH. Instead of solving a global linear system for compatibility, the position of SPH nodes are adapted so that compatibility conditions are naturally enforced using classical and well-known SPH gradients.

In the context of Lagrangian simulation, this means that the SPH nodes are not advected with the physical velocity, but with a corrected velocity. The idea is not new: it can be traced back to Monaghan and his XSPH formulation [19], and appeared more recently in the context of fluid dynamics with the works of Adami, Hu and Adams ([1] and [16] for instance). In this work, we try to incorporate their corrections to our framework, generalize their method and give a novel interpretation for their results.

1 INTRODUCTION

Smoothed Particle Hydrodynamics (SPH) is a family of meshless simulation methods initiated in 1977 with the independent contributions of Lucy ([17]) and Gingold and Monaghan ([10]). SPH was initially applied to astrophysical problems and still enjoys success in this field (see [25] for a recent review), but its scope of applications soon widened to cover very complex flow problems ([11] for fluid-structure interaction for instance, [2] regarding chemically reacting viscous flows), elasticity and plasticity problems ([18] for instance), as well as complex magneto-hydrodynamic problems ([24]). Thanks to its robustness, SPH seems ideally suited to give an answer to geometrically or physically complex problems, where all other methods usually fail. Comparatively little work has been dedicated to solve well established simple test-cases with analytical solutions (let us cite [13] and [3] as exceptions).

However, SPH has long suffered from stability issues characterized by local loss of quality of the point cloud (particle clumping, formations of voids. See for instance [26] where the infamous term ”tensile instability” originated) Unsurprisingly, the main effort in the SPH community has been to propose several remedies to control the apparition of instability (see [19] with the XSPH formulation and [20] introducing artificial stress formulation). More recently, significant improvements to stability as well as point-wise accuracy have been achieved with Adami, Hu and Adams’ ”transport-velocity” formulation (see [1] and [16]).

In previous works ([21] and [22]), the present authors have investigated the influence of the properties of discrete meshless differentiation operators (or meshless ”gradients”) on the accuracy of the solution of a simple diffusion problem in the context of nodal integration. In section 2, we very briefly recall the symmetric meshless discretization of the diffusion problem and derive sufficient conditions to pass the patch test, which we call ”compatibility conditions”. Our earlier work [22] focused on the recovery of these conditions via the modification of gradient coefficients and the introduction of a corrected gradient at the cost of solving a global linear system. Section 2.6 however is an attempt to achieve compatibility while keeping the computational simplicity of SPH: Instead of solving a global linear system for compatibility, the position of SPH nodes are adapted so that compatibility conditions are naturally enforced using classical and well-known SPH gradients. We show that this technique yields second order convergence for the diffusion problem.

Finally, we revisit the contributions of Adami, Hu and Adams and propose a slightly different procedure to limit the inconsistencies of the classical SPH gradient. This modification allows an easier interpretation and exploration of its consequences, which we undertake in section 3.

2 DISCRETIZATION OF THE DIFFUSION PROBLEM

2.1 The Meshless Framework

In SPH, every node i of the point cloud $\mathcal{C}$ (including those of the ”boundary” cloud $\partial\mathcal{C}$) located at coordinates $\mathbf{x}_i$ is attributed a positive volume usually denoted V_i. These volumes play the role of weights to define a discrete scalar product between fields $f, g : \mathcal{C} \rightarrow \mathbb{R}$, approximating the classical L^2 scalar product between functions as:

$$(f, g)_{\mathcal{C}} = \sum_{i \in \mathcal{C}} V_i f_i g_i \tag{1}$$

A discrete meshless differential operator, or ”meshless gradient” is a linear operator $\mathbb{V}$: $(\mathcal{C} \rightarrow \mathbb{R}) \rightarrow (\mathcal{C} \rightarrow \mathbb{R}^d)$ that maps a scalar field $f : \mathcal{C} \rightarrow \mathbb{R}$ to a vector field $\mathbb{V} f : \mathcal{C} \rightarrow \mathbb{R}^d$ (d is the number of space dimensions). Such an operator can always be written at point i as:

$$V_i \mathbb{V}_i f = \sum_{j\in\mathcal{C}} \mathbf{A}_{i,j} f_j \tag{2}$$

where the $\mathbf{A}_{i,j}$ are vector coefficients (the coefficient V_i was added for convenience, see equation 4). There is *a priori* (and in general) no relation between $\mathbf{A}_{i,j}$ and $\mathbf{A}_{j,i}$.

A meshless gradient is said to have n-th order consistency if it is exact on all monomials of order at most n. Mimicking integration by parts theorem, given a "primal" meshless gradient $\mathbb{V}$, we can introduce a "dual" meshless gradient $\mathbb{V}^*$, as:

$$\forall f, g : \mathcal{C} \to \mathbb{R} \mid f_{\partial\mathcal{C}} = 0, \quad (\mathbb{V} f, g)_{\mathcal{C}} + (f, \mathbb{V}^* g)_{\mathcal{C}} = 0 \tag{3}$$

Remark: We only consider functions that are identically null on the border $\partial\mathcal{C}$ not to have to include a boundary term in the right-hand side of equation 3. Boundary nodes will thus need to receive a special treatment in what follows.

From equation 3, we can easily derive that the coefficients $\mathbf{A}^*_{i,j}$ of the dual gradient will in general read:

$$\forall i, j \in \mathcal{C} \quad \mathbf{A}^*_{i,j} = -\mathbf{A}_{j,i} \tag{4}$$

The (skew-)symmetry of this formula entails $\mathbb{V}^{**} = \mathbb{V}$. This underlines the fact that $\mathbb{V}$ and $\mathbb{V}^*$ are actually dual to each other. There is *a priori* no reason to prefer one gradient over the other.

2.2 Classical examples of meshless gradients

Given a kernel function W_h, let us list three well-known meshless gradient from the SPH literature (see [14]) as well as their dual counterparts:

- The "classical" SPH gradient, which is equal to its dual because of the symmetry properties of the kernel function:

$$\mathbb{V}_i^{\mathrm{CLASS}} f = -\sum_{j\in\mathcal{C}} V_j \nabla W_h(\mathbf{x}_j - \mathbf{x}_i) f_j \tag{5}$$

- The renormalized gradient of order 0, which is zeroth-order consistent:

$$\mathbb{V}_i^{\mathrm{R0}} f = -\sum_{j\in\mathcal{C}} V_j \nabla W_h(\mathbf{x}_j - \mathbf{x}_i)(f_j - f_i) \tag{6}$$

  Its dual gradient can be written as:

$$\mathbb{V}_i^{\mathrm{R0}*} f = -\sum_{j\in\mathcal{C}} V_j \nabla W_h(\mathbf{x}_j - \mathbf{x}_i)(f_j + f_i) \tag{7}$$

  In particular, the dual renormalized 0 gradient of a constant scalar field is twice the classical gradient of this constant : $\mathbb{V}^{\mathrm{R0}*}1 = 2\mathbb{V}^{\mathrm{CLASS}}1$.

- The renormalized gradient of order 1:

$$\mathbb{V}_i^{\mathrm{R1}} f = -\sum_{j\in\mathcal{C}} V_j \mathbb{B}_i \nabla W_h(\mathbf{x}_j - \mathbf{x}_i)(f_j - f_i) \tag{8}$$

Where $\mathbb{B}_i$ is the $d \times d$ matrix set as to recover first order consistency:

$$\mathbb{B}_i^{-1} = \mathbb{V}_i^{\mathrm{R0}}\mathbf{x} = -\sum_{j \in \mathcal{C}} V_j \nabla W_h(\mathbf{x}_j - \mathbf{x}_i) \otimes (\mathbf{x}_j - \mathbf{x}_i) \tag{9}$$

In the above formula, $\otimes$ denotes the classical tensor product. The dual gradient $\mathbb{V}_i^{\mathrm{R1}*}$ can be written:

$$\mathbb{V}_i^{\mathrm{R1}*} f = -\sum_{j \in \mathcal{C}} V_j(\mathbb{B}_i f_i + \mathbb{B}_j f_j) \nabla W_h(\mathbf{x}_j - \mathbf{x}_i) \tag{10}$$

2.3 Strong discretization of the diffusion problem

In the following sections, regularity conditions which should be put on continuous fields are knowingly ignored because they are irrelevant to the discretization procedure.
Let us consider the following strong form of the diffusion problem with Dirichlet boundary conditions on $\Omega \subset \mathbb{R}^d$:

$$\begin{cases} -\Delta u = s \\ u|_{\partial\Omega} = g \end{cases} \tag{11}$$

If we bluntly replace continuous operators with discrete ones, we find the following strong SPH discretization:

$$\begin{cases} -\mathbb{V}_i \cdot \mathbb{V} u = s_i & \forall i \in \mathcal{C} \\ u_i = g_i & \forall i \in \partial\mathcal{C} \end{cases} \tag{12}$$

Note that this is not the only possible meshless discretization of the strong form given in equation 11. Equation 12 defines the following strong discrete Laplace operator:

$$(-\mathbb{\Delta})_{i,j} = (-\mathbb{V} \cdot \mathbb{V})_{i,j} = -\sum_{k \in \mathcal{C}} \frac{\mathbf{A}_{i,k} \cdot \mathbf{A}_{k,j}}{V_i V_k} \tag{13}$$

This operator is not symmetric in general, has been observed to yield nearly singular systems, and thus would need stabilization techniques in order to give satisfactory results. A sufficient condition for the discrete strong laplacian of a linear function to identically vanish (which is a sufficient condition for the patch test) is the first order consistency of the meshless gradient $\mathbb{V}$.

2.4 Weak discretization of the diffusion problem

The corresponding weak form of the diffusion problem can be written as follows: $\forall v : \Omega \to \mathbb{R} \mid v|_{\partial\Omega} = 0$,

$$\begin{cases} \displaystyle\int_\Omega \nabla u \cdot \nabla v = \int_\Omega sv \\ u|_{\partial\Omega} = \quad g \end{cases} \tag{14}$$

Again bluntly replacing continuous operators with discrete ones, we find the following weak SPH discretization: $\forall v : \mathcal{C} \to \mathbb{R} \mid v|_{\partial\mathcal{C}} = 0$,

$$\begin{cases} (\mathbb{V}u, \mathbb{V}v)_{\mathcal{C}} = (s, v)_{\mathcal{C}} \\ u|_{\partial\Omega} = \quad g \end{cases} \tag{15}$$

The coefficients of the corresponding (self-adjoint !) weak laplacian discrete operator then read:

$$(-\mathbb{\Delta})_{i,j} = (-\mathbb{V}^* \cdot \mathbb{V})_{i,j} = \sum_{k \in \mathcal{C}} \frac{\mathbf{A}_{k,i} \cdot \mathbf{A}_{k,j}}{V_i V_k} \tag{16}$$

Sufficient conditions for the discrete weak laplacian of a linear function to be null (which is a necessary condition for the patch test) are the first order consistency of the primal gradient $\mathbb{V}$ **and** the zeroth-order consistency of the dual gradient $\mathbb{V}^*$. This second condition, which we call compatibility is paramount: it involves both discrete integration and discrete differentiation and can be re-stated (via equation 3) as a discrete version of Stokes' theorem. None of the gradients described in section 2.2 naturally enforces this condition on general clouds of points. In the meshless literature, the notion of compatibility appeared in the work of Bonet (see [3]), where compatibility is sought by means of kernel correction. The second notable contribution is Chiu's in [4]. However, Chiu does not discriminate between primal and dual gradients since he *a priori* enforces skew-symmetry of his gradient coefficients.

Our previous work [22] showed that using a corrected version of the renormalized 1 gradient, it is possible to experience second order convergence rate for the diffusion problem with sources. More importantly, it also suggested that exact compatibility is not strictly necessary for second-order convergence: it seems sufficient to bound the term $\|\mathbb{V}^* 1\|$ with a constant as the point cloud is refined instead of the worst-case $\|\mathbb{V}^* 1\| = \mathcal{O}(h^{-1})$ (Here, h denotes a typical inter-particular distance in the point cloud. It is chosen proportional to the maximum distance $\|\mathbf{x}_j - \mathbf{x}_i\|$ for which either $\mathbf{A}_{i,j}$ or $\mathbf{A}_{j,i}$ is non-null). We call these gradients ”quasi-compatible”.

In section 2.6, we will once again demonstrate that using a first order consistent and quasi-compatible gradient yields ultimate second order convergence for the diffusion problem.

2.5 Another symmetric discretization of the diffusion problem

Inspired by finite volume discretizations on orthogonal meshes, other discretizations of the diffusion operator have also been proposed in the meshless literature (see [7] for a review SPH discretizations of the diffusion operator). The details vary, but the most promising (according to [7]) reads in coefficients:

$$(-\mathbb{\Delta})_{i,j} = 2V_j \frac{\nabla W_h(\mathbf{x}_j - \mathbf{x}_i) \cdot (\mathbf{x}_j - \mathbf{x}_i)}{\|\mathbf{x}_j - \mathbf{x}_i\|^2} \quad \forall i \neq j \in \mathcal{C} \tag{17}$$

This operator is self-adjoint and the related bi-linear form reads:

$$\langle f, g \rangle_{\mathcal{C}} = \sum_{i,j \in \mathcal{C}} V_i V_j \frac{\nabla W_h(\mathbf{x}_j - \mathbf{x}_i) \cdot (\mathbf{x}_j - \mathbf{x}_i)}{\|\mathbf{x}_j - \mathbf{x}_i\|^2} (f_j - f_i)(g_j - g_i) \tag{18}$$

The conditions for the patch test can once again be restated as compatibility conditions. Indeed in the case of the above laplacian (using a kernel with radial symmetry), a sufficient condition for the laplacian of a linear field to vanish is that the classical (dual) gradient of the unit field $\mathbb{V}^{\mathrm{CLASS}} 1$ vanishes.

2.6 Looking for quasi-compatible configurations and results

The generation of point clouds well-suited for meshless simulations is somehow similar to the meshing procedure in mesh-based methods: it should not be performed regardless of the numerical method that follows. Generating point cloud has recently been an active area of research in the computer graphics community, where harmonious yet unstructured point clouds are sought. Several methods to build these "blue noise" configuration bear striking similarities with the method exposed here. See [8], [12] and [5] for more details.

In [1] and [16], Adami, Hu and Adams add a "background pressure" source term to their momentum equation as the gradient of a constant field. This term was demonstrated to have a regularizing effect on the point cloud, which gave better approximation properties to the underlying kernel estimation of (constant in their incompressible setting) density.
In order to better understand this source term, let us define the following function of all the node coordinates:

$$\mathcal{V} = \sum_{i,j \in \mathcal{C}} V_i V_j W_h(\mathbf{x}_j - \mathbf{x}_i) \tag{19}$$

Let us remark that $\mathcal{V}$ is non-negative and thus admits at least a minimum on every compact.

The gradient of $\mathcal{V}$ with respect to $\mathbf{x}_k$ can be written:

$$\frac{\partial \mathcal{V}}{\partial \mathbf{x}_k} = -2V_k \sum_{j \in \mathcal{C}} V_j \nabla W_h(\mathbf{x}_j - \mathbf{x}_k) = V_k \mathbb{\nabla}^{R0*} 1 \tag{20}$$

Hence, this constant pressure source term (eq. 17 of [16]) can be re-written using our notations:

$$2 \sum_j V_i V_j \nabla W_h(\mathbf{x}_j - \mathbf{x}_i) P_c = -V_i \mathbb{\nabla}_i^{R0*} P_c = -P_c \frac{\partial \mathcal{V}}{\partial \mathbf{x}_i} \tag{21}$$

Since their second term is dissipative (it is the discretization of viscosity forces), their procedure can be thought of as a generalized gradient descent trying to minimize $\mathcal{V}$. They remain unclear concerning the boundary condition that were used, but we can safely assume that there were either fixed nodes surrounding the discretized domain or that periodic boundary conditions were used. In any case, the $\mathbf{x}_j$ are bound to rest in a compact region, and a local minimum of $\mathcal{V}$ is ultimately reached. This local minimum has zero gradient, hence it defines a point cloud where the discrete dual meshless gradient of a constant function is null. With such node positions, the classical gradient is compatible (and consistent, and coincides with the renormalized 0 gradient).

Similarly, we generated several clouds of points of different sizes using a gradient descent algorithm. The algorithm was stopped when the norm of the gradient of a unit field reached a given threshold. We call this threshold "Stokes' default" since it is a measure of how much Stokes' formula fails to be satisfied. We also tried the same procedure using the renormalized 1 gradient. Even if we could not find any function similar to $\mathcal{V}$ which partial derivatives with respect to positions give the dual gradient of a constant function, we still have been able to reduce $||\mathbb{\nabla}^* 1||$ by three orders of magnitude or more using this technique.

In our tests, the nodes were initially distributed as a low discrepancy Halton sequence (see [9] for details about low discrepancy sequences), and two layers of boundary nodes ensured that no particle escaped the simulation domain. These particles were later used to enforce Dirichlet boundary conditions for the diffusion equation. Node volumes were chosen all equal, and so that their sum reproduced the volume of the simulation domain. This is in agreement with the Quasi-Monte Carlo philosophy associated with low discrepancy sequences. Typical node arrangements are displayed on figures 1 to 4.

Concerning the diffusion equations, the source s and the Dirichlet border conditions are set so that an analytical solution is known. Thus, it was possible to perform an h-convergence analysis for each presented gradient. The corresponding curves are shown in figures 7 - 9. On each curve, the Stokes default is kept below the following thresholds: 100, 50, 30, 10, 5, 3, 1, 0.5 and 0.3. It should be clear from these curves that enforcing compatibility conditions is a good means to improve accuracy of diffusion simulations. Indeed, the lower the Stokes default, the best the accuracy. With poor compatibility, very poor accuracy was consistently obtained (error $\geq 100\%$) for all gradients.

It can also be noted that increasing the order of consistency of the primal gradient was always beneficial to accuracy. Finally let us remark that only the first order consistent gradient produced straight-looking accuracy curves. A linear least-squares fit of the three last curves (Stokes default 1, 0.5 and 0.3) gave approximate order of convergence of 2.03, 2.08 and 2.10. This is why we claim we achieve ultimate second order convergence if we keep the Stokes default under a low enough threshold.

3 APPROXIMATE ADVECTION AND COMPATIBILITY

In the context of Lagrangian simulation, the point cloud is evolving at every time step. In this section, we will show on a concrete example that exact advection of the nodes along the physical velocity field is not a desirable feature of a SPH simulation. The idea is not new, and several authors have proposed regularized velocity fields better suited for advection ([19] and his XSPH formulation is probably the most famous). To a large extend, artificial viscosity can also be regarded as an additional source in the momentum equation.

It is often not clear how the addition of those regularizing source terms impact the kinematics of the fluid. This section quantatively explores the implications of the use of an ALE velocity on the mean level of Stokes default.

3.1 An ALE source term

Corrective procedures proposed in [19] (XSPH), [1] (transport-velocity) and [15] (Fick-diffusion based regularization) are difficult to analyze because they are directly formulated at the time-discretized level. Hence, time discretization and space discretization are already coupled, and it is quite often not clear how they really interact. This is the reason why we propose an Arbitrary Lagrangian Eulerian (see [6] for a good introduction to ALE formulations) velocity formulation independent of the time discretization. In the results that we show, high order time discretization as well as low time steps were used so that time discretization errors are completely negligible.

Let us suppose that the space discretization is initially very good, and that the computed velocity field $\mathbf{v}(\mathbf{x})$ is extremely close to the physical velocity. In order to go to the next time-step, the simulation procedure should carry the SPH nodes along the streamlines of the velocity for the duration of a time-step. Figure 10 shows the advection of initially regularly arranged nodes after advection with a Taylor-Green flow (which is a solution of the incompressible Navier-Stokes equations). Even if the flow is extremely regular (in our example it is smooth and its divergence is zero, thus not creating voids or excess of fluid in any area at the continuous level), we can see that, at a discrete level, holes have been created in some areas, and nodes have clumped in others. Concurrently, the Stokes default (as plotted on figure 15) quickly rises from a null value (the cartesian arrangement of nodes is compatible), to a size-dependant small range of values (40-50 in the example). At mid-time, the flow velocity is reversed and the flow travels back towards the initial state. Symmetry of figure 15 demonstrates the time-reversibility of the approach.

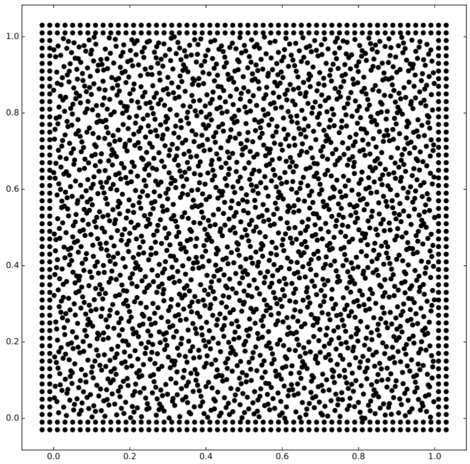

Figure 1: Halton sequence of 2500 nodes

$\|\nabla^{\mathrm{CLASS}*}1\| \approx 14.5$

$\|\nabla^{\mathrm{R0}*}1\| \approx 29.1$

$\|\nabla^{\mathrm{R1}*}1\| \approx 36.3$

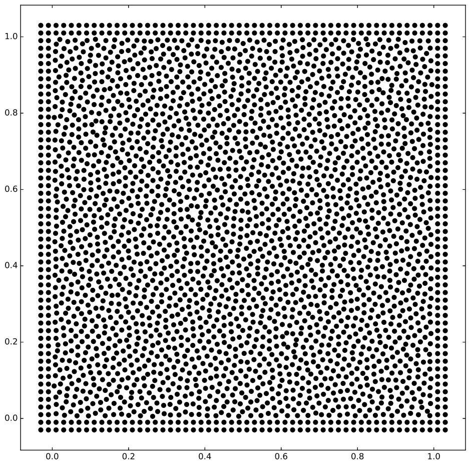

Figure 2: Modified point cloud. $\|\nabla^{\mathrm{CLASS}*}1\| \approx 1$

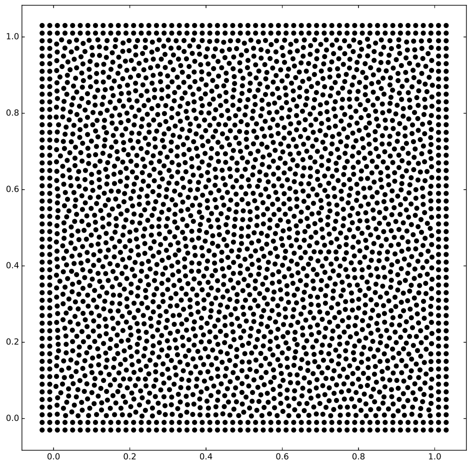

Figure 3: Modified point cloud. $\|\nabla^{\mathrm{R0}*}1\| \approx 1$

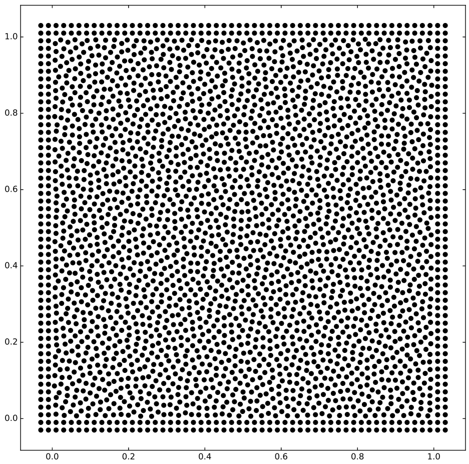

Figure 4: Modified point cloud. $\|\nabla^{\mathrm{R1}*}1\| \approx 1$

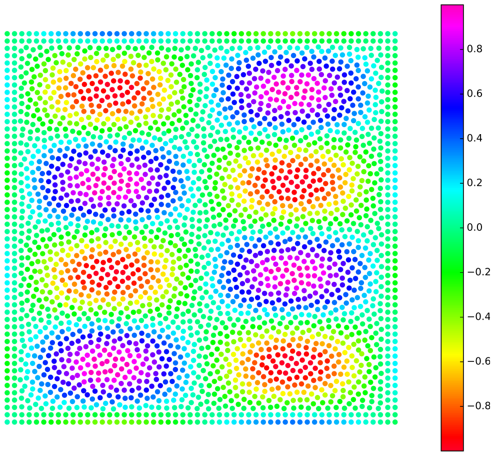

Figure 5: SPH solution using the renormalized 1 gradient

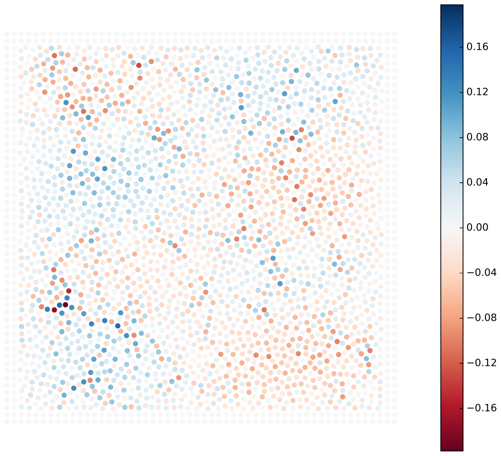

Figure 6: Signed error to exact solution

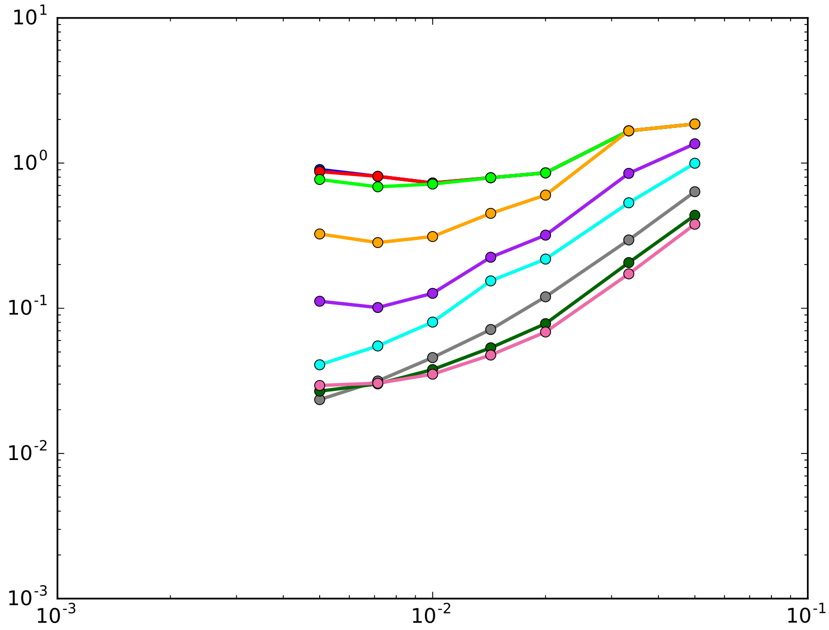

Figure 7: Relative error of the laplacian system as a function of discretization length for the classical gradient with Stokes default kept below 100, 50, 30, 10, 5, 3, 1, 0.5 and 0.3

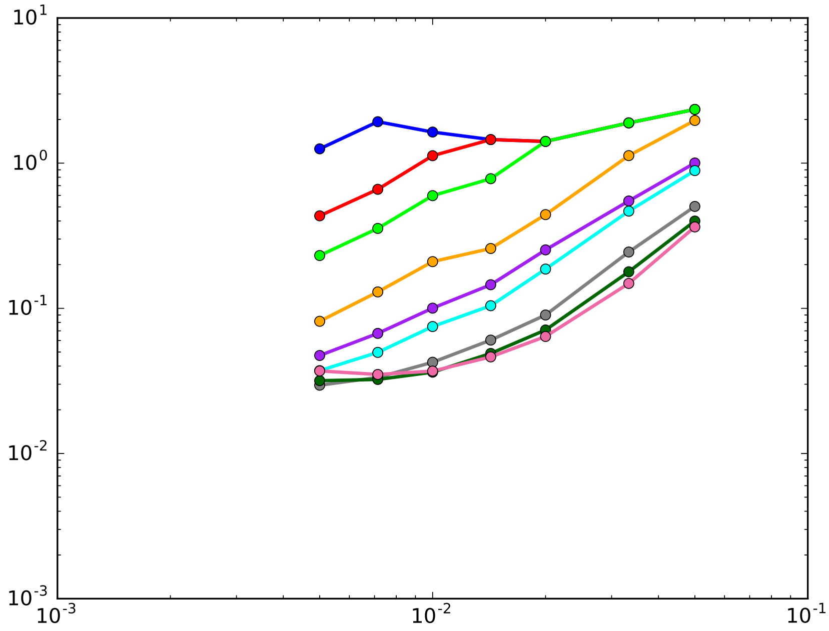

Figure 8: Relative error of the laplacian system as a function of discretization length for the renormalized 0 gradient with Stokes default kept below 100, 50, 30, 10, 5, 3, 1, 0.5 and 0.3

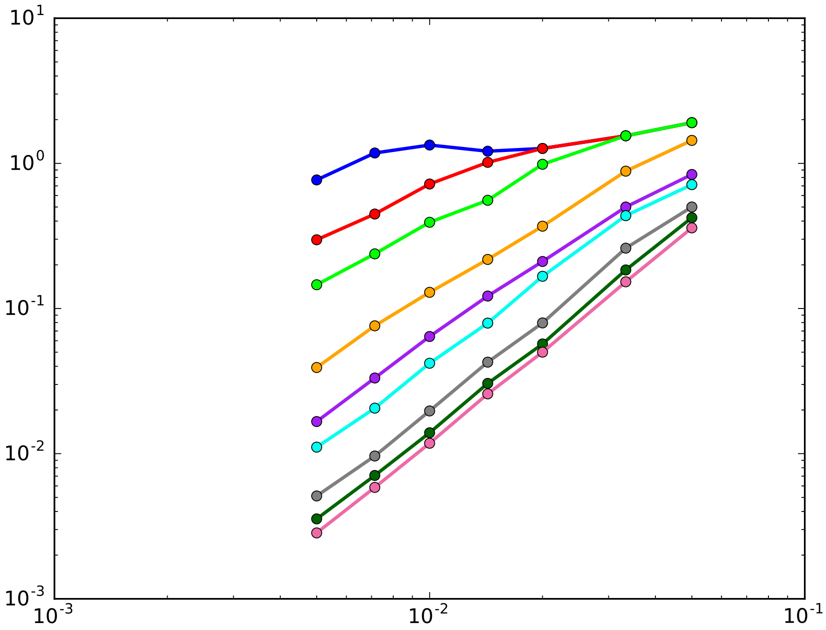

Figure 9: Relative error of the laplacian system as a function of discretization length for the renormalized 1 gradient with Stokes default kept below 100, 50, 30, 10, 5, 3, 1, 0.5 and 0.3.

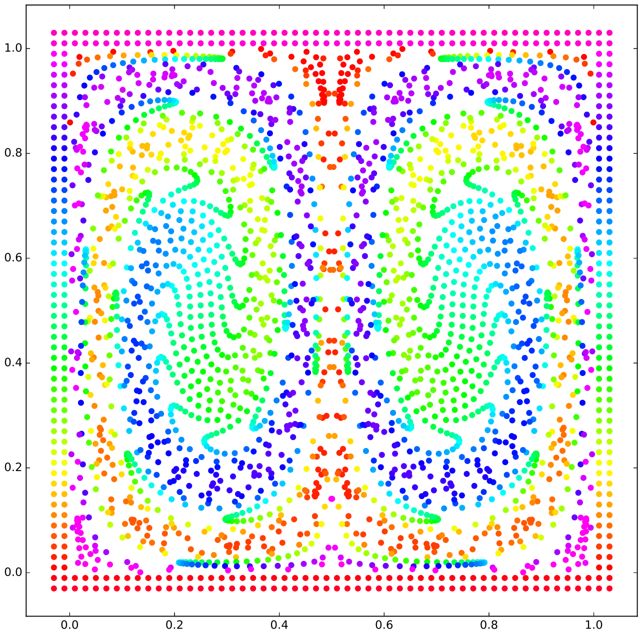

Figure 10: Advection of initially regular cloud of 2500 nodes by the Taylor-Green vortex flow. The color of each particle is set as a function of is initial y-coordinate. The two outer layers of nodes were kept fixed

In order to create figure 10, the following uncoupled system of ODEs was solved:

$$\frac{\mathrm{d}\mathbf{x}_i}{\mathrm{d}t} = \mathbf{v}(\mathbf{x}_i) \quad \forall i \in \mathcal{C} \tag{22}$$

While equation 22 defines the solution of the exact node advection, we could instead seek a ”close” solution to the advection problem while keeping a better mesh quality (i.e. lower Stokes default). For instance, we could solve the following system (where $\mathbf{c}_i$ is a ”small” velocity field designed so as to keep the Stokes default under a given threshold).

$$\frac{\mathrm{d}\mathbf{x}_i}{\mathrm{d}t} = \mathbf{v}(\mathbf{x}_i) - \mathbf{c}_i \quad \forall i \in \mathcal{C} \tag{23}$$

In 23, $\mathbf{c}_i$ can immediately be interpreted as the ALE velocity defined in [6] in the context of point cloud advection (as opposed to mesh advection).
Inspired by the quasi-gradient descent method of [16], we propose the following easy to compute expression for $\mathbf{c}_i$ (where γ is a user-provided constant):

$$\mathbf{c}_i = \gamma \mathbb{V}_i^* 1 \tag{24}$$

All the presented results used the classical SPH gradient $\mathbb{V}^{\mathrm{CLASS}}$, but extremely similar results were obtained with the renormalized 1 gradient $\mathbb{V}^{\mathrm{R1}}$. Figure 17 shows the time evolution of the mean Stokes default as a function of time when integrating system 23 - 24 with several values of the parameter γ. The velocity field $\mathbf{v}$ is again chosen to be the Taylor-Green vortex flow (reversed after $t = 50$). We can see that the value of the mean Stokes default quickly stabilizes at a near-constant level. This level depends on the total number of simulation nodes as well as the parameter γ as pictured in figures 18 - 20.

Least-square fitting in figures 18 and 20 reveal the following approximate dependencies: $\|\mathbb{V}^{\mathrm{CLASS}*}1\| \propto \gamma^{-0.65} h^{0.35}$ when $\gamma \neq 0$, whereas the ALE speed grows as: $\|\mathrm{c}_i\| = \gamma \|\mathbb{V}^{\mathrm{CLASS}*}1\| \propto \gamma^{0.35} h^{0.35}$. Of course, these exponents are probably case-dependent, but they still seem to indicate that one could choose a value $\gamma = \mathcal{O}(\sqrt{h})$ in order to keep $\|\mathbb{V}^{\mathrm{CLASS}*}1\| = \mathcal{O}(1)$. This choice would ensure that the advection velocity goes to zero as the cloud is refined as $\|\mathrm{c}_i\| = \mathcal{O}(\sqrt{h})$, so that the method is asymptotically Lagrangian instead of fully ALE. Of course, other compromises could also be made.

As a final remark, let us note that using formulation 23 - 24 with gradient$\mathbb{V}^{\mathrm{CLASS}*}$lowers the value of $\|\mathbb{V}^{\mathrm{R1}*}\|$ for a given value of the parameter γ, but this value still increases as h increases as shown in figure 19. This fact slightly tempers the good results presented in [15].

4 CONCLUSIONS AND FUTURE WORK

In section 2.1 we presented a meshless framework for the discretization of partial differential equations and gave the example of the diffusion equation. In section 2.4, we studied the patch test using a symmetric discretization of the diffusion equation underlining the key role of the so-called compatibility conditions, a discrete counterpart of Stokes’ formula. In section 2.6 , we showed that good accuracy of the solution to the discrete laplacian problem could not be reached unless the compatibility conditions were met at least approximately.

In section 3 we linked previously proposed stabilization techniques with the recovery of a quasi-compatible gradient. We also proposed a new procedure to enforce approximate compatibility in ALE simulations.

In future works, we would like to investigate the role of the discretization of the boundary (meshed boundaries, ghost particles, . . .) on the ALE formulation we proposed and extend the

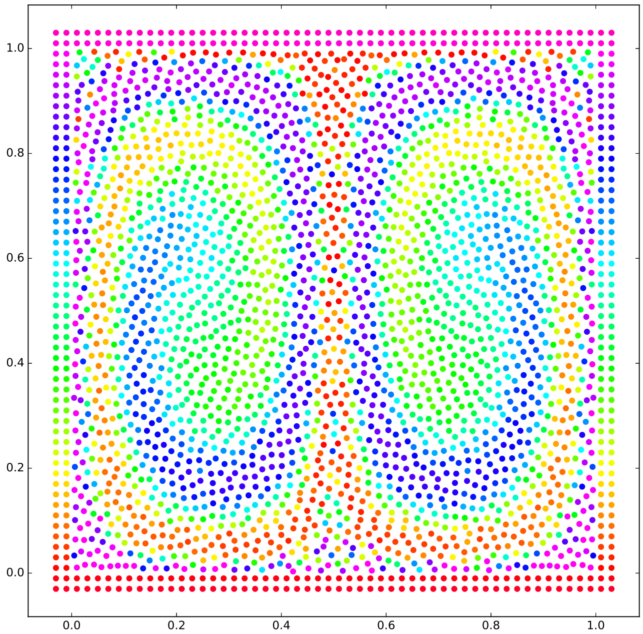

Figure 11: Advection of initially regular cloud of 2500 nodes by the Taylor-Green vortex flow using formulation 23 - 24 with $\gamma = 0.003$ at time $t = 50$ (mid-time). The color of each particle is set as a function of is initial y-coordinate. The two outer layers of nodes were kept fixed

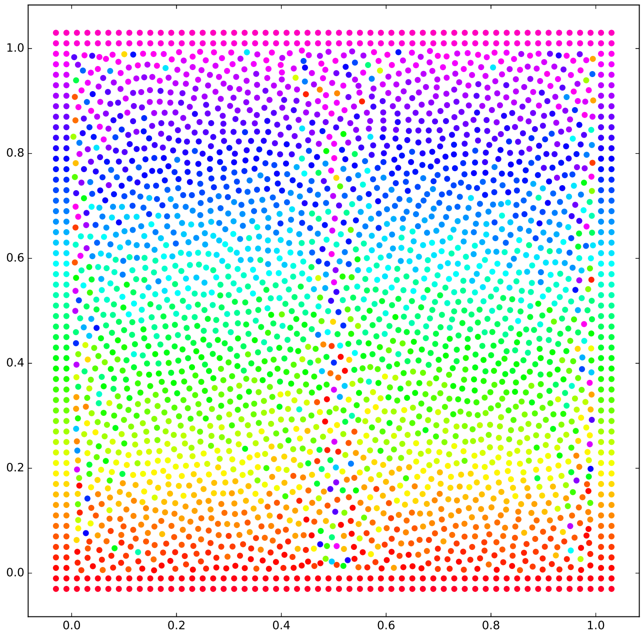

Figure 12: Advection of initially regular cloud of 2500 nodes by the Taylor-Green vortex flow using formulation 23 - 24 with $\gamma = 0.003$ at time $t = 100$ (end-time). The color of each particle is set as a function of is initial y-coordinate. The two outer layers of nodes were kept fixed. The error compared to exact avection can be visually appreciated with the non-uniformity of the color field.

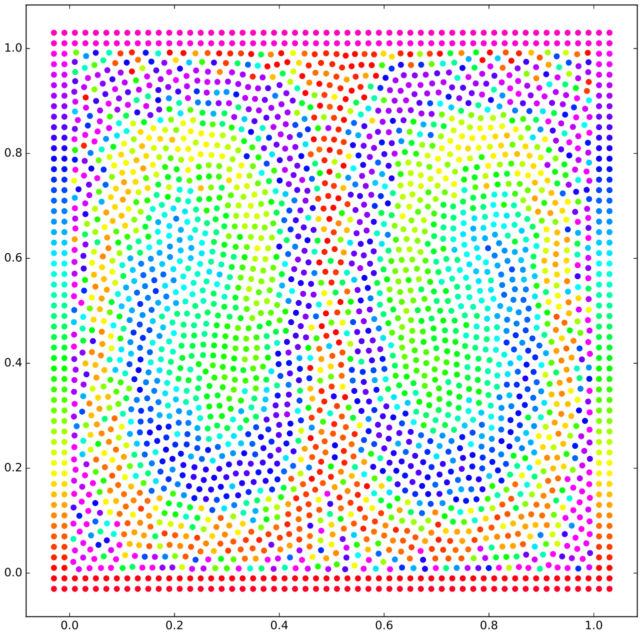

Figure 13: Advection of initially regular cloud of 2500 nodes by the Taylor-Green vortex flow using formulation 23 - 24 with $\gamma = 0.1$ at time $t = 50$ (mid-time). The color of each particle is set as a function of is initial y-coordinate. The two outer layers of nodes were kept fixed

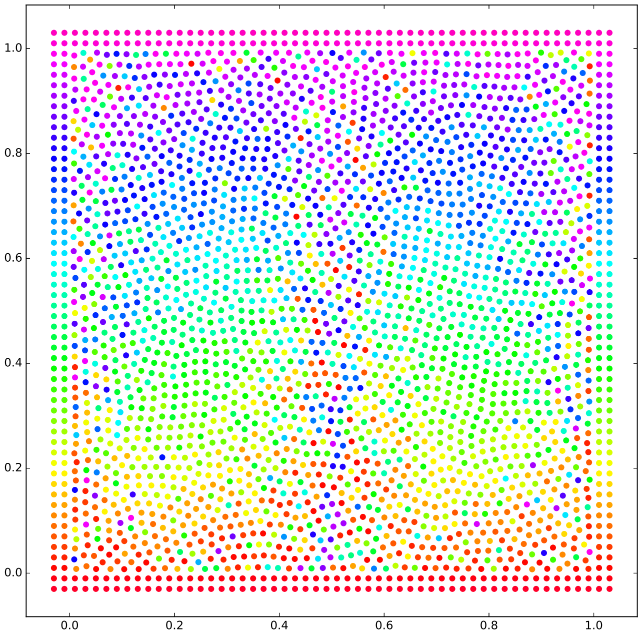

Figure 14: Advection of initially regular cloud of 2500 nodes by the Taylor-Green vortex flow using formulation 23 - 24 with $\gamma = 0.1$ at time $t = 100$ (end-time). The color of each particle is set as a function of is initial y-coordinate. The two outer layers of nodes were kept fixed. The error compared to exact avection can be visually appreciated with the non-uniformity of the color field.

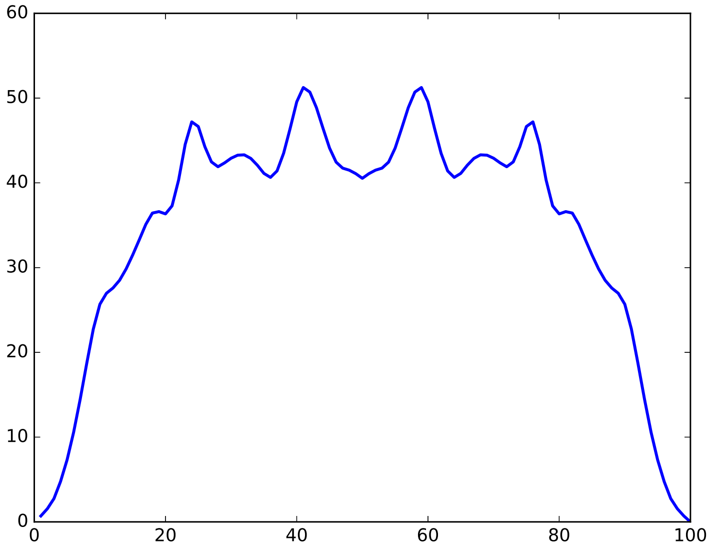

Figure 15: Mean Stokes default of an initially regular cloud of 2500 nodes advected by the Taylor-Green vortex flow as a function of time. At time $t = 50$, the flow is reversed (hence the symmetry of the curve)

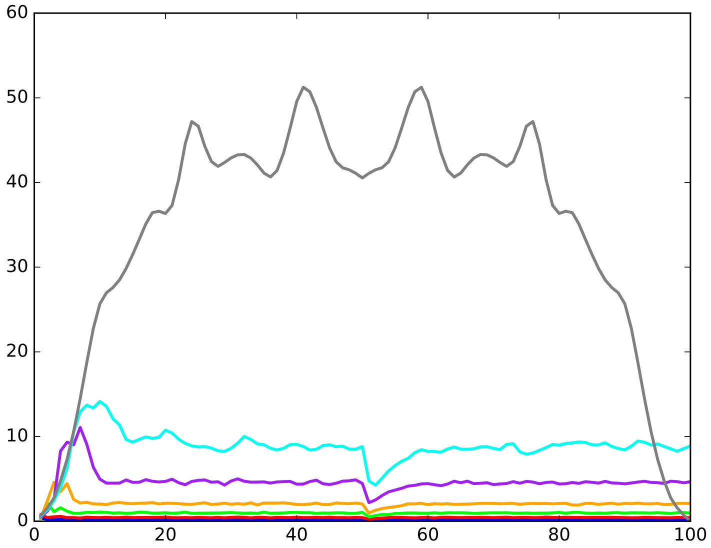

Figure 16: Mean Stokes default of an initially regular cloud of 2500 nodes advected by the Taylor-Green flow, and relaxed by formulations 23 - 24 as a function of time. At time $t = 50$, the Taylor-Green flow is reversed, but the ODE system is no longer time-reversible. The values of γ used are: 0.3, 0.1, 0.03, 0.01, 0.003, 0.001 and 0.

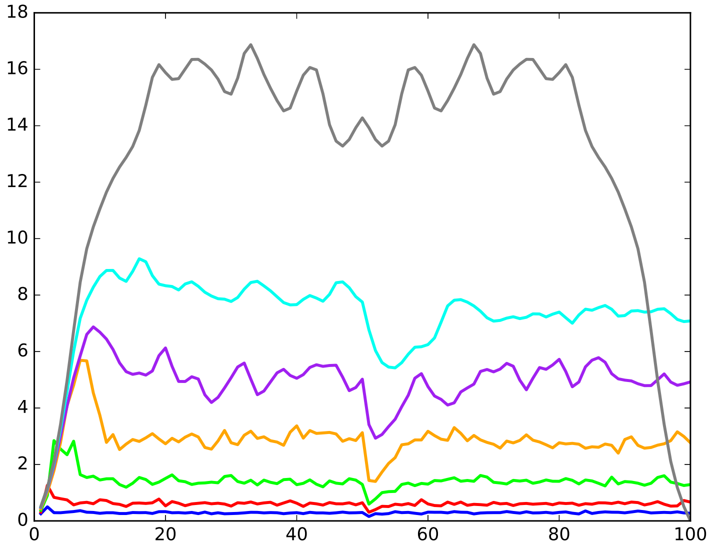

Figure 17: Mean Stokes default of an initially regular cloud of 400 nodes advected by the Taylor-Green flow, and relaxed by formulations 23 - 24 as a function of time. At time $t = 50$, the Taylor-Green flow is reversed, but the ODE system is no longer time-reversible. The values of γ used are: 0.3, 0.1, 0.03, 0.01, 0.003, 0.001 and 0.

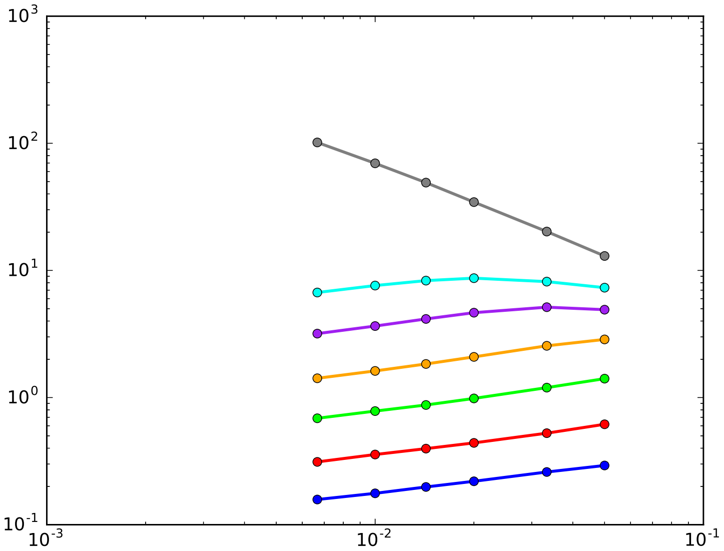

Figure 18: Averaged mean Stokes default as a function of discretization length in the case of the Taylor-Green vortex flow relaxed by formulation 23 - 24. The values of γ used are: 0.3, 0.1, 0.03, 0.01, 0.003, 0.001 and 0.

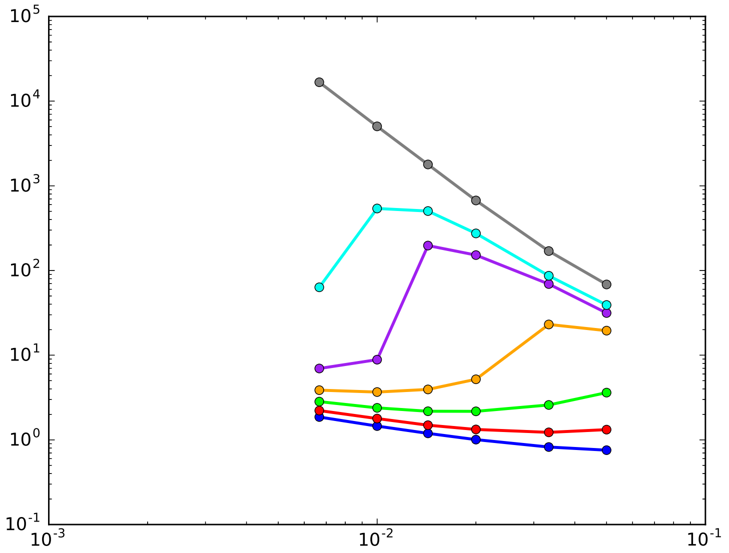

Figure 19: Averaged mean Stokes default of gradient $\mathbb{V}^{\mathrm{R1}}$ as a function of discretization length, when using gradient $\mathbb{V}^{\mathrm{CLASS}}$ in 23 - 24. The values of γ used are: 0.3, 0.1, 0.03, 0.01, 0.003, 0.001 and 0.

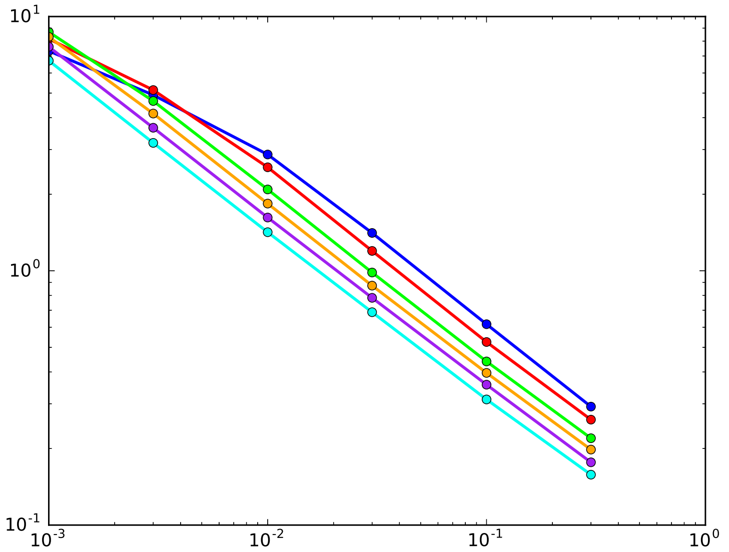

Figure 20: Averaged mean Stokes default as a function of the parameter γ in the case of the Taylor-Green vortex flow relaxed by formulation 23 - 24. The number of nodes used are: 400, 900, 2500, 4900, 10000 and 22500

analysis to more complicated simulations (fluid flows for instance, but also structural mechanics). Additionally, we would like to clarify the role of the functional $\mathcal{V}$ defined in equation 19 and generalize its definition to other gradients.

REFERENCES

[1] S. Adami, X.Y. Hu, and N.a. Adams. A transport-velocity formulation for smoothed particle hydrodynamics. *Journal of Computational Physics*, 241:292–307, 2013.

[2] a.K. Chaniotis, D. Poulikakos, and P. Koumoutsakos. Remeshed Smoothed Particle Hydrodynamics for the Simulation of Viscous and Heat Conducting Flows. *Journal of Computational Physics*, 182(1):67–90, 2002.

[3] J Bonet and S Kulasegaram. Correction and stabilization of smooth particle hydrodynamics methods with applications in metal forming simulations. *International Journal for Numerical Methods in Engineering*, 47(July 1998):1189–1214, 2000.

[4] Edmond Kwan-yu Chiu. *A Conservative Meshless Framework for Conservation Laws with Applications in Computational Fluid Dynamics*. PhD thesis, Stanford University, 2011.

[5] Fernando de Goes, Katherine Breeden, Victor Ostromoukhov, and Mathieu Desbrun. Blue noise through optimal transport. *ACM Transactions on Graphics*, 31(6):1, 2012.

[6] J Donea, Antonio Huerta, J Ponthot, and a Rodr. Arbitrary Lagrangian Eulerian Methods. *Encyclopedia of Computational Mechanics*, pages 1–25, 1999.

[7] R Fatehi and M T Manzari. Error estimation in smoothed particle hydrodynamics and a new scheme for second derivatives. *Computers Math.\ Applic.*, 61:482–498, 2011.

[8] Raanan Fattal. Blue-noise point sampling using kernel density model. *ACM Transactions on Graphics*, 30(4):1, 2011.

[9] Henri Faure, Peter Kritzer, and Friedrich Pillichshammer. From van der Corput to modern constructions of sequences for quasi-Monte Carlo rules. *Indagationes Mathematicae*, 26(5):760–822, 2015.

[10] R. A. Ginghold and J.J. Monaghan. Smoothed particle hydrodynamics : theory and application to non-spherical stars. *Monthly Notices of the Royal Astronomical Society*, 181:375–389, 1977.

[11] PM Guilcher. *Contribution au développement d'une méthode SPH pour la simulation numérique des interactions houle-structure*. PhD thesis, Université de Nantes, 2008.

[12] Min Jiang, Yahan Zhou, Rui Wang, Richard Southern, and Jian Jun Zhang. Blue noise sampling using an SPH-based method. *ACM Transactions on Graphics*, 34(6):1–11, 2015.

[13] Nathalie Lanson. *Etude des méthodes particulaires renormalisées. Applications aux problèmes de la dynamique rapide.* PhD thesis, INSA, 2001.

[14] Nathalie Lanson and Jean-Paul Vila. Renormalized Meshfree Schemes I: Consistency, Stability, and Hybrid Methods for Conservation Laws, 2008.

[15] S. J. Lind, R. Xu, P. K. Stansby, and B. D. Rogers. Incompressible smoothed particle hydrodynamics for free-surface flows: A generalised diffusion-based algorithm for stability and validations for impulsive flows and propagating waves. *Journal of Computational Physics*, 231(4):1499–1523, 2012.

[16] S. Litvinov, X.Y. Hu, and N.a. Adams. Towards consistence and convergence of conservative SPH approximations. *Journal of Computational Physics*, 301:394–401, 2015.

[17] L. B. Lucy. A numerical approach to the testing of the fission hypothesis. *The astronomical journal*, 82(12):1013–1024, 1977.

[18] Bertrand Maurel. *Modélisation par la méthode SPH de l'impact d'un réservoir rempli de fluide*. PhD thesis, INSA Lyon, 2008.

[19] J.J. Monaghan. On the problem of penetration in particle methods. *Journal of Computational Physics*, 82(1):1–15, 1989.

[20] J.J. Monaghan. SPH without a Tensile Instability. *Journal of Computational Physics*, 159(2):290–311, apr 2000.

[21] Guillaume Pierrot. Meshless methods: a unified framework and analysis. In *ESI Expert Seminar on Meshless Methods*, 2011.

[22] Guillaume Pierrot and Gabriel Fougeron. Enforcing differentiation/integration compatibility in meshless methods with nodal integration. In *Particle-based Methods IV Fundamentals and Applications*, 2015.

[23] Guillaume Pierrot and Gabriel Fougeron. Discrete gradient theorem and element-based integration in meshless methods. *VII European Congress on Computational Methods in Applied Sciences and Engineering*, 2016.

[24] Daniel J Price. Smoothed Particle Hydrodynamics and Magnetohydrodynamics. *J. Comp. Phys.*, 231:759–794, 2012.

[25] Volker Springel. Smoothed Particle Hydrodynamics in Astrophysics. *ARAA*, 48(1), 2010.

[26] JW Swegle, DL Hicks, and SW Attaway. Smoothed Particle Hydrodynamics Stability Analysis. *Journal of Computational Physics*, 116(1):123–134, 1995.